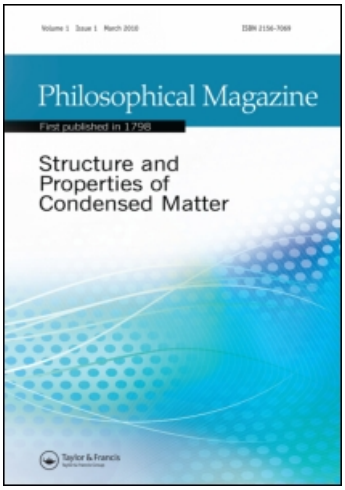

Philosophical Magazine
Publication details, including instructions for authors and subscription information:
http://www.informaworld.com/smpp/title~content=t713695589

Smaller is tougher

A. R. Beaber[a]; J. D. Nowak[b]; O. Ugurlu[c]; W. M. Mook[d]; S. L. Girshick[e]; R. Ballarini[f]; W. W. Gerberich[a]
[a] Department of Chemical Engineering and Materials Science, University of Minnesota, Minneapolis, MN 55455, USA [b] Hysitron Incorporated, Minneapolis, Minnesota 55344, USA [c] Characterization Facility, University of Minnesota, Minneapolis, MN 55455, USA [d] Laboratory for Mechanics of Materials and Nanostructures, Empa - Materials Science & Technology, CH-3602 Thun, Switzerland [e] Department of Mechanical Engineering, University of Minnesota, Minneapolis, MN 55455, USA [f] Department of Civil Engineering, University of Minnesota, Minneapolis, MN 55455, USA

First published on: 25 June 2010

To cite this Article Beaber, A. R. , Nowak, J. D. , Ugurlu, O. , Mook, W. M. , Girshick, S. L. , Ballarini, R. and Gerberich, W. W.(2011) 'Smaller is tougher', Philosophical Magazine, 91: 7, 1179 — 1189, First published on: 25 June 2010 (iFirst)
To link to this Article: DOI: 10.1080/14786435.2010.487474
URL: http://dx.doi.org/10.1080/14786435.2010.487474

Philosophical Magazine
Vol. 91, Nos. 7–9, 1–21 March 2011, 1179–1189

Taylor & Francis
Taylor & Francis Group

Smaller is tougher

A.R. Beaber[a]*, J.D. Nowak[b], O. Ugurlu[c], W.M. Mook[d], S.L. Girshick[e], R. Ballarini[f] and W.W. Gerberich[a]

[a]*Department of Chemical Engineering and Materials Science, University of Minnesota, 421 Washington Ave SE, Minneapolis, MN 55455, USA;* [b]*Hysitron Incorporated, 10025 Valley View Road, Minneapolis, Minnesota 55344, USA;* [c]*Characterization Facility, University of Minnesota, Minneapolis, MN 55455, USA;* [d]*Laboratory for Mechanics of Materials and Nanostructures, Empa – Materials Science & Technology, Feuerwerkstr. 39, CH-3602 Thun, Switzerland;* [e]*Department of Mechanical Engineering, University of Minnesota, 111 Church St SE, Minneapolis, MN 55455, USA;* [f]*Department of Civil Engineering, University of Minnesota, 500 Pillsbury Dr SE, Minneapolis, MN 55455, USA*

(*Received 19 November 2009; final version received 15 April 2010*)

"Smaller is stronger" is now a tenet generally consistent with the predominance of evidence. An equally accepted tenet is that fracture toughness almost always decreases with increasing yield strength. Can "smaller is tougher" then be consistent with these two tenets? It is taught in undergraduate engineering courses that one design parameter that allows for both increased strength and fracture toughness is reduced grain size. The present study on the very brittle semiconductor silicon proves this exception to the rule and demonstrates that smaller can be both stronger and tougher. Three nanostructures are considered theoretically and experimentally: thin films, nanospheres, and nanopillars. Using a simple work per unit fracture area approach, it is shown at small scale that toughness is inversely proportional to the square root of size. This is supported by experimental evidence from *in situ* electron microscopy nanoindentation at length scales of less than a micron. It is further suggested that dislocation shielding can explain both strength and toughness increases at the small scales.

Keywords: *in situ* nanoindentation; fracture toughness; brittle–ductile transition; silicon; fracture mechanics; nanoparticle

1. Introduction

Recent results on evaluations of nanowires, atomic force microscopy (AFM) tips, nanospheres, and nanopillars strongly suggest a size dependence in fracture resistance [1–6]. Much of this has been based on observations of a size-dependent fracture toughness of silicon [1,2,7]. Most recently, it was shown that by decreasing size alone, the brittle to ductile transition in silicon could be reduced from 800 K to 300 K by simply reducing size to the vicinity of a couple of hundred nanometers [2]. Whereas this was by compressing pillars, it is nevertheless significant since bulk

*Corresponding author. Email: beaber@cems.umn.edu

ISSN 1478–6435 print/ISSN 1478–6443 online

DOI: 10.1080/14786435.2010.487474
http://www.informaworld.com

silicon under indentation is brittle with toughness in the vicinity of 0.8 MPa $m^{1/2}$. This caused us to further examine the fracture toughness of silicon nanospheres with *in situ* transmission electron microscopy (TEM). One such result to be discussed later is shown in Figure 1. The first abrupt unloading is commensurate with fracture. Other results giving a hint to a size related ductile–brittle transition temperature were given earlier by Nakao et al. [8], where a factor of two increase in fracture toughness was observed for 4 μm thick beams at about 70°C (see Figure 2).

As most of the previous fractures observed did not result in arrested cracks, it was decided to evaluate additional silicon spheres and pillars with the analysis technique being a work per unit fracture area or J-integral technique. A couple of in-depth analyses of silicon nanopillar fractures [2] that did arrest provides an evaluation of this hypothesis. Since fracture toughness had been previously correlated to impact energies or slow-notch-bend energy release rates, the underlying hypothesis is that the work done is largely released in this relatively brittle solid. In the first part of the paper, fracture toughness for volumes limited in one, two, and three dimensions will be discussed in terms of work per unit fracture area. This is followed by a more precise discrete dislocation approach for silicon nanospheres and nanopillars.

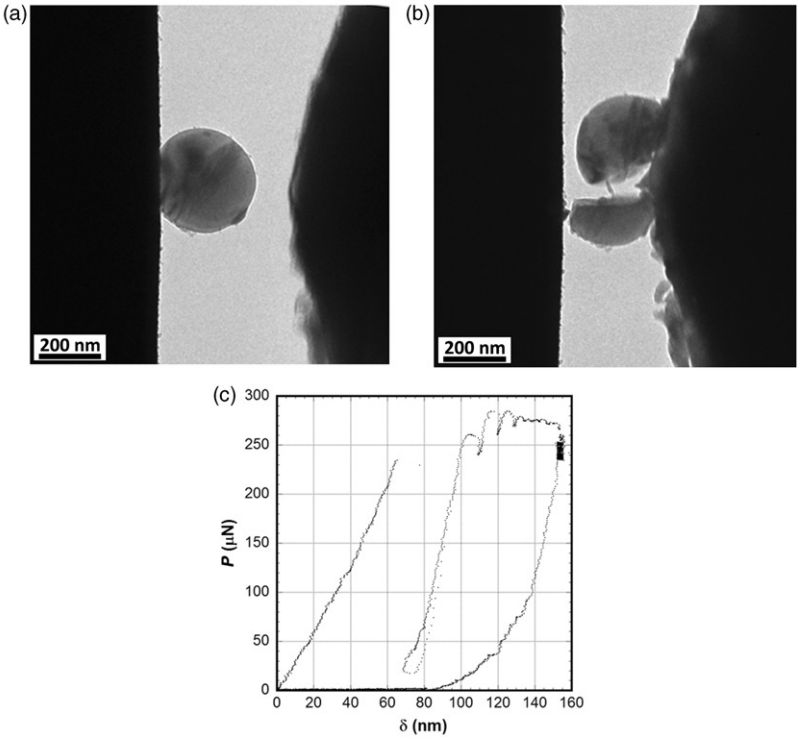

Figure 1. *In situ* fracture in a TEM of a 349 nm diameter silicon nanosphere under displacement control at 10 nm/s. (a, b) Nanosphere before and after indentation. (c) Load–displacement curve showing fracture at 230 μN, followed by a rapid load drop and reloading to give additional plasticity.

2. Work/unit fracture area (W/A)

The concept here is little different than a Charpy V-notch (CVN) bar where the impact energy divided by the fracture area (W/A) represents the strain energy release rate, G_{Ic}, in J/m^2. Schematically, the concept for films, spheres, and pillars is represented by the work to deform the volume surrounding the area which fractures releasing stored energy. These are depicted in Figure 3. For very ductile materials, the CVN correlations to toughness take into account that a certain amount of energy

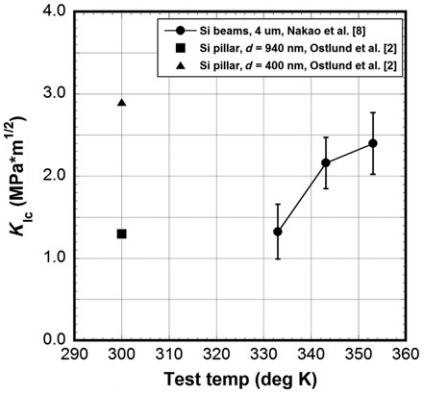

Figure 2. Fracture toughness from 4 μm thick silicon single crystal beams in bending (Nakao et al. [8]) and silicon pillars in compression (Ostlund et al. [2]) as a function of test temperature.

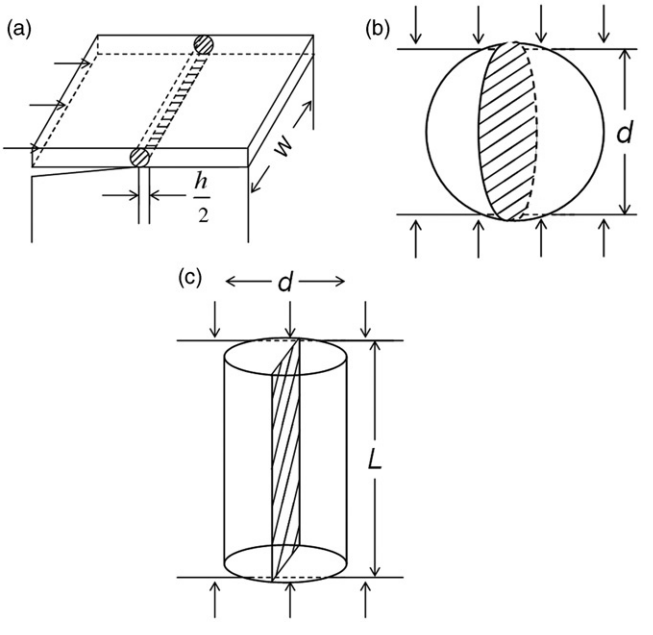

Figure 3. Work/unit fracture area schematics for (a) films of thickness h and width w; (b) spheres of diameter d; and (c) pillars of height L and diameter d.

is required to initiate the crack. Because these nanostructures sustain such high stresses prior to fracture, the assumption here is that almost any 5 nm surface step or imperfection will represent a natural crack. For the majority of cases posed in this study, the assumption will be that the W/A relates to crack propagation energy. In integrating the plastic work for relatively brittle fracture, we have assumed a plastic volume noted by the shaded region in Figures 3a–3c. This is considered to experience a yield stress and a plastic strain equivalent to the yield strain. Any increased plasticity could be satisfied by increasing the constant k.

2.1. *Thin films*

Considering W/A, the work associated with a cylindrical plastic volume (see Figure 3a) undergoing yield is

$$W = \pi\left(\frac{h}{2}\right)^2 w \int \sigma \, \mathrm{d}\varepsilon. \tag{1a}$$

This represents the deforming volume times the strain energy density, with h and w the film thickness and width, respectively. For relatively brittle delamination of thin films where interfacial energies are small, this simplifies by taking the stress to yield, σ_{ys}, and a yield strain, $\varepsilon = \sigma_{ys}/E$. Thus, the work becomes

$$W = \frac{\pi h^2 w}{4} \frac{k^2}{h^2 E}, \tag{1b}$$

if film yield stress is taken as kh^{-1} rather than $kh^{-1/2}$ as in the Hall–Petch solution. For small length scales, there is some evidence that an h^{-1} dependence is appropriate. Since the area swept out under this volume is wh, one finds

$$\frac{W}{A} \simeq \frac{\pi k^2}{4hE}. \tag{2}$$

Furthermore, the strain energy release rate is related to fracture toughness, K_{Ic}, through $K_{Ic} = [EG_{Ic}]^{1/2}$, giving

$$K_{Ic} \simeq k[\pi/4h]^{1/2}, \tag{3}$$

noting that k has units of N/m and ignoring any Poisson ratio effect if this were truly plane strain. Also note that a Hall–Petch scaling of the yield stress would lead to a size independent solution.

2.2. *Nanospheres*

With a volume of $\frac{4}{3}\pi\left(\frac{d}{2}\right)^3$ and the same estimate of strain energy density, one finds that

$$W = \frac{4}{3}\pi\left(\frac{d}{2}\right)^3 \frac{k^2}{d^2 E}. \tag{4}$$

As indicated in Figure 2b, the fracture area, A, would be $\pi d^2/4$ so that

$$G_{\mathrm{Ic}} = \frac{W}{A} \simeq \frac{2}{3}\frac{k^2}{dE}. \tag{5}$$

Similarly this converts to

$$K_{\mathrm{Ic}} \simeq k\left[\frac{2}{3d}\right]^{1/2}, \tag{6}$$

nearly identical to Equation (3) for the thin film case.

2.3. *Nanopillars*

For nanopillars in compression, this is less definitive due to the different height to diameter ratios possible. Here, it is assumed that the typical height, h, is approximately $4d$ to prevent buckling. As above for the strain energy density times the volume,

$$W = \frac{\pi d^2}{4} 4d \frac{k^2}{d^2 E}, \tag{7}$$

using the height, L, to be $4d$. For a vertical crack traversing the length of the pillar, the area is Ld or $4d^2$ in the case of buckling avoidance. This gives

$$G_{\mathrm{Ic}} = \frac{W}{A} \simeq \frac{\pi k^2}{4dE}. \tag{8}$$

Using the same conversion to fracture toughness yields

$$K_{\mathrm{Ic}} \simeq k\left[\frac{\pi}{4d}\right]^{1/2}. \tag{9}$$

It is remarkable that Equations (3), (6), and (9) are nearly identical to the fracture toughness inversely proportional to the square root of the critical length scale. In the following, this is explored with both previous and new experimental findings.

3. Experimental procedures and results

Thin film and nanopillar data [1,2] are taken from previously published results where the testing procedures are outlined. The major exception is the nanosphere tests where previous fracture toughness procedures on spheres in the range of 40–200 nm in diameter used oxide film thickness as a measure of the critical crack size [7,9]. It is now becoming apparent that this underestimates the fracture toughness as it was only an elastic estimate of the stress intensity factor. Generally, the spheres experience a considerable amount of plasticity prior to fracture. As the W/A approach here still might be underestimating toughness, it is proposed that this is nevertheless a more realistic estimate of strain energy release rate. In the recent work, where both methods were utilized, G_{Ic} values taken from plasticity considerations had toughness about two times to five times greater than the more conservative

estimate. As the higher values were more consistent with nanopillars where finite element and analytical solutions were possible, this approach will be used here.

3.1. *Thin films*

From previous studies of thin film nanoindentation and delamination [10], it was determined that the yield strength for film thickness and hence grain size could be given by [11]

$$\sigma_{ys} = \sigma_o\left[1 + \gamma h^{-1/2}\right], \tag{10}$$

which is like a Hall–Petch relationship except that h is film thickness, $\sigma_o = 400\,\text{MPa}$ and $\gamma = 0.287\,\mu\text{m}^{-1/2}$ for copper thin films. Additionally, a blocked slip band model related to polycrystalline fracture, utilized dislocation shielding concepts for semibrittle polycrystals, as given by [12,13]

$$K_{Ic} = \alpha\sigma_{ys}\sqrt{\frac{d}{\pi}} + \frac{\beta\mu b}{\sigma_{ys}\sqrt{d}}, \tag{11}$$

where d is the grain size, μb the shear modulus times the Burgers vector, and α and β are unknown coefficients. For relatively coarse-grained materials, α was taken as unity but for ultra-fine grains or very thin films α would be greater. With $\alpha = 3$ and $\beta = 2 \times 10^{10}\,\text{MPa}$, the fit to previous thin film data [10] for copper is shown in Figure 4. Even though the prediction is not particularly good, it does give the decrease in toughness with increasing film thickness at large thicknesses. Also, the minimum in toughness is in the vicinity of that observed. By choosing an appropriate value of k one could also use an inverse thickness dependence that would give the

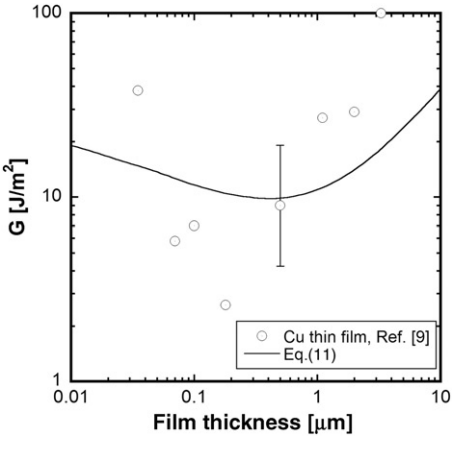

Figure 4. Strain energy release rate of Cu films bonded to Si with a thin 8 nm Ti layer. A top layer of added W to store elastic energy produced buckling upon nanoindentation. Data from Volinsky et al. [10]. Solid curve represents a dislocation shielding model for low energy fracture or delamination from Huang and Gerberich [12] and Katz et al. [13]. Note that the error bar is for triplicate results.

correct yield strength for a 200 nm thick film. However, this would appear to overestimate the yield strength at 30 nm. Still, at much smaller film thicknesses the constraint would raise the flow stress considerably. For example, the hardness of a 200 nm sputter-deposited Au film increased from 4.5 to 6 GPa with increasing penetration and a 660 nm evaporated and annealed Au film increased from 0.5 to 1.5 GPa due to the increased constraint with increasing depth [14]. If you assumed k as above and used an inverse film thickness dependence, along with appropriate values for α and β in Equation (11), a slope matching the small thickness data in Figure 4 could be obtained. As sufficient data were not available, such a calculation was not conducted.

Previously, for the larger thickness regime, it was considered that toughness only increased with film thickness due to the global plastic energy dissipation in thicker and lower yield strength films [15,16]. Frank et al.'s [17] observations of increased toughness for very small film thicknesses caused us to reexamine the previously unexplained Cu data shown at the smallest thicknesses in Figure 4. Our tentative explanation is that dislocation shielding at a blocked boundary (the second term in Equation (11)) and the global plastic energy dissipation (the first term in Equation (11)) dictate the minimum observed.

3.2. *Nanosphere strength*

Two sets of experimental data for single crystal silicon spheres are presented in Figure 5. The first, published elsewhere, are from Mook et al. [7] based upon an AFM/nanoindentation system (Hysitron Triboscope), which allowed load–displacement under load and imaging of residual displacement after unloading. As discussed elsewhere, this allowed for contact stresses to be measured with plastic displacements utilized to estimate strains and dislocation activity [7]. Similarly, *in situ* experiments in a 120 kV FEI Tecnai T12 transmission electron microscope were conducted for the

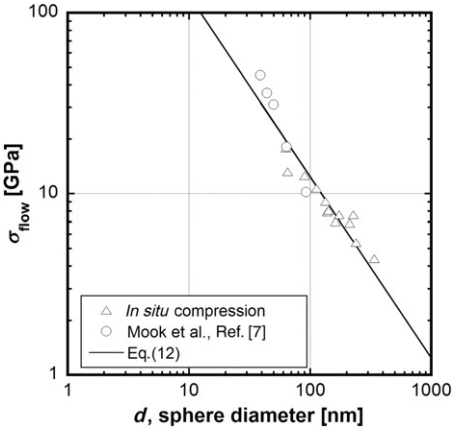

Figure 5. Strength of silicon spheres in compression as a function of diameter based on *in situ* AFM/nanoindentation and *in situ* TEM load–displacement curves. Solid curve is Equation (12) based upon proposed linear hardening model.

present study. This also used a diamond tip with a MEMS-based transducer (Hysitron PicoIndenter), an example being shown in Figure 1. Experiments were run in displacement control with loading/unloading rates of 10 nm/s. Maximum stresses are reported here based on the assumption that the back stress of emitted dislocations requires an ever increasing stress to either nucleate dislocations from the same source or even nucleate dislocations from a parallel source. Evidence to this effect in silicon is from reversed plasticity observations in nanospheres [18] and recent atomistic simulations using a classic Stillinger–Weber potential [19], which realistically represents elasticity and cohesive forces. This had previously led to a linear hardening model for constrained thin films and for spheres becoming [20,21]

$$\sigma_{\text{flow}} = \frac{2\mu N_{\text{eff}} b}{\pi(1-\nu)d}, \tag{12}$$

where μ is the shear modulus, b the Burgers vector, ν is Poisson's ratio of silicon, and d is the sphere diameter. To be elaborated upon more fully in the discussion section, both the data from the AFM and TEM systems are well-represented by the linear hardening model of Equation (12).

3.3. *Nanosphere and pillar toughness*

Prior nanosphere fractures are detailed previously with vertical fractures similar to those in Figure 1 being detected by atomic force microscopy scanning [7]. There, several estimates of fracture toughness based upon either the average measured oxide thickness or a work per unit fracture area were presented [7]. These tended to underestimate the plasticity contributions by a factor of two to five as they were conservative elasticity-based. Here, we use a J-integral based determination for a sphere as given by

$$J = \frac{\int P\,\mathrm{d}\delta}{A}. \tag{13}$$

Using the values given in Table 1 of Mook et al. [7] for load, displacement and area, this gives the values of $K_{\text{Ic}} = [EJ]^{1/2}$ shown in Figure 6. Current *in situ* TEM

Table 1. Work per unit fracture determinations of spheres and pillars.

	Diameter (nm)	Height (nm)	P (mN)	δ (nm)	J (N/m)	K_{Ic} (MPa m$^{1/2}$)
Spheres	349	–	235	74	91	3.81
	280	–	320	72	185	5.45
	255	–	265	70	188	5.5
	206	–	190	72	203	5.6
Towers[a]	113	–	87	53	230	6.1
	415	532	260	75	72	3.4
	325	500	370	42.5	94.7	3.9
	231	665	95	113	128	4.5

Notes: [a]These towers failed through the diameter rather than vertically. These were ⟨111⟩ orientation as opposed to prior vertical fractures in the ⟨100⟩ orientation which failed along c planes.

evaluations using the same method for those spheres that were taken to failure are given in Table 1 and also shown in Figure 6. Additionally, several spheres and pillars were analyzed using both a work per unit fracture area and a finite element analysis procedure described in detail elsewhere [2,7]. The three somewhat bigger towers tested in our laboratories had relatively small aspect ratios of 1.5 to 2.9 resulting in little possibility of buckling. Also evaluated with Equation (13), the details for these are also given in Table 1. Besides these towers, two additional towers of ⟨100⟩ orientation focus-ion-beam machined (FIB) out of wafers were analyzed in detail with both analytical and finite element determination of toughness. Nevertheless, all data fell roughly on the same curve, demonstrating a more gradual size effect in Figure 6 compared to that for strength in Figure 5. The solid curve model in Figure 6 for fracture toughness is discussed below.

4. Discussion and summary

Previous results have suggested that constrained thin films provide higher hardness due to a linear hardening mechanism [21]. This led to Equation (12) for nanospheres, which is also relevant to constrained plastic flow of nanopillars. Regarding thin films, the measured delamination toughness increases by about a decade as thickness decreases by a decade (see Figure 4). This is larger than the inverse square root dependence suggested by Equation (3), but any difference could be associated with the scarcity of data and the large error bars. One should be aware, however, that the 'error' bar is due to a resistance-curve effect as all indentation-induced blisters were not the same size. Qualitatively, then, the fracture toughness represented by the dislocation shielding argument in Equation (11) is largely controlled by the thickness which is Equation (3) from the simple W/A argument.

One can be more confident in the single crystal, initially dislocation free, silicon spheres and nanopillars, where there is an absence of microstructural effects.

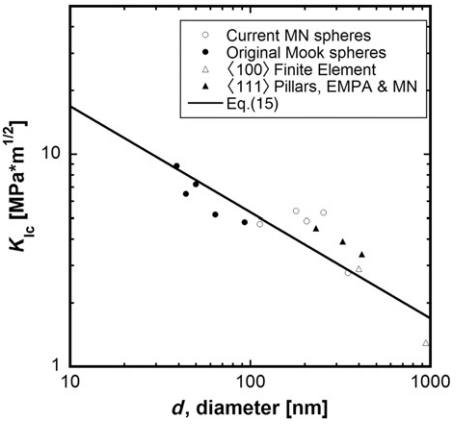

Figure 6. Fracture toughness of silicon spheres and pillars showing that smaller is tougher. Solid curve is Equation (15) based upon the linear hardening model and the dislocation shielding concept of Equation (11).

By relating the linear dislocation hardening model of Equation (12) to the same dislocation shielding argument of Equation (11), one can arrive at a size-scale dependent fracture toughness relationship. It had originally been shown that a dislocation shielding equation could be derived for 15 oxides, nitrides, and semiconductors, given by [22]

$$K_{\mathrm{Ic}} = \frac{10}{9}\left[\frac{N\mu\sigma_{\mathrm{ys}}b}{1-\nu}\right]^{1/2}, \tag{14}$$

where N is the number of shielding dislocations. The slightly different prefactor compared to [22] is due to using a more exact solution. This was applied to fracture toughness results predominately determined by indentation into single crystals or large-grained polycrystals. For small volumes under much higher stresses, where the modulus may be increased due to the hydrostatic component of stress, N is taken as N_{eff} and the other variables are taken as bulk values with σ_{ys} as the maximum stress in Figure 5. This allows the use of Equation (12) to eliminate yield stress from Equation (14) giving

$$K_{\mathrm{Ic}} = \frac{10}{9}\mu N_{\mathrm{eff}}\, bd^{-1/2}, \tag{15}$$

which is the solid curve in Figure 6. It is clear that an inverse square-root size dependence is consistent with this data set if N_{eff} remains the same. One can rationalize this as dislocations would be packed together more closely the smaller the size scale, particularly at a shielded crack tip with a pile-up blocked by a boundary. That is, the smaller size promotes higher strength with the higher stress more closely packing the dislocations. Due to the far field applied stress as well as the crack-tip stress field interacting with all dislocations, it is not surprising that the length scale functionally for toughness is different than that found for the strength. Still, these results can only be considered as provisional and await more in-depth atomistic and discretized simulations as well as additional experimental results. It is also tempting to believe that the original work per unit fracture concepts resulting in Equations (3), (6), and (9) are realistic in that they are consistent with the inverse square root dependence of Equation (15). Whatever the final result, there is now evidence that not only is smaller stronger, but also smaller is tougher.

Acknowledgements

This work was supported by the National Science Foundation (CTS-0506748), the Air Force Office of Scientific Research (AOARD-08-4134), and the Abu Dhabi–Minnesota Institute for Research Excellence (ADMIRE), a partnership between the Petroleum Institute (PI) of Abu Dhabi and the Department of Chemical Engineering and Materials Science of the University of Minnesota. Parts of this work were carried out in the Institute of Technology Characterization Facility, University of Minnesota, a member of the NSF-funded Materials Research Facilities Network (www.mrfn.org).

References

[1] W.W. Gerberich, J. Michler, W.M. Mook, R. Ghisleni, F. Östlund, D.D. Stauffer and R. Ballarini, J. Mater. Res. 24 (2009) p.898.
[2] F. Östlund, K. Rzepiejewska-Malyska, K. Leifer, L.M. Hale, Y. Tang, R. Ballarini, W.W. Gerberich and J. Michler, Adv. Funct. Mater. 19 (2009) p.2439.
[3] M. Kopycinska-Mueller, R.H. Geiss and D.C. Hurley, MRS Proc. 924 (2006) p.19.
[4] B. Moser, K. Wasmer, L. Barbieri and J. Michler, J. Mater. Res. 22 (2007) p.1004.
[5] X. Han, K. Zheng, Y. Zhang, X. Zhang, Z. Zhang and Z.L. Wang, Adv. Mater. 19 (2007) p.2112.
[6] T.Y. Kim, S.S. Han and H.M. Lee, Mater. Trans. 45 (2004) p.1442.
[7] W.M. Mook, J.D. Nowak, C.R. Perrey, C.B. Carter, R. Mukherjee, S.L. Girshick, P.H. McMurry and W.W. Gerberich, Phys. Rev. B 75 (2007) p.214112.
[8] S. Nakao, T. Ando, M. Shikida and K. Sato, J. Micromech. Microeng. 18 (2008) p.1.
[9] J.D. Nowak, W.M. Mook, A.M. Minor, W.W. Gerberich and C.B. Carter, Phil. Mag. A 87 (2007) p.29.
[10] A.A. Volinsky, N.R. Moody and W.W. Gerberich, Acta Mater. 50 (2002) p.441.
[11] Y. Wei and J.W. Hutchinson, J. Mech. Phys. Solid 45 (1997) p.1137.
[12] H. Huang and W.W. Gerberich, Acta Metall. Mater. 40 (1992) p.2873.
[13] Y. Katz, R. Keller, H. Huang and W. Gerberich, Metall. Mater. Trans. A 24 (1993) p.343.
[14] M.J. Cordill, D.M. Hallman, N.R. Moody, D.P. Adams and W.W. Gerberich, Metall. Mater. Trans. A 38 (2007) p.2154.
[15] M.D. Kriese, N.R. Moody and W.W. Gerberich, Acta Mater. 46 (1998) p.6623.
[16] M. Lane, R.H. Dauskardt, N. Krishna and I. Hashim, J. Mater. Res. 15 (2000) p.203.
[17] S. Frank, U.A. Handge, S. Olliges and R. Spolenak, Acta Mater. 57 (2009) p.1442.
[18] W.W. Gerberich, W.M. Mook, M.J. Cordill, C.B. Carter, C.R. Perrey, J.V.R. Heberlein and S.L. Girshick, Int. J. Plast. 21 (2005) p.2391.
[19] F.H. Stillinger and T.A. Weber, Phys. Rev. B 31 (1985) p.5262.
[20] J.D. Nowak, A.R. Beaber, O. Ugurlu, S.L. Girshick and W.W. Gerberich, Scripta Mater. 62 (2010) p.819.
[21] M.J. Cordill, M.D. Chambers, M.S. Lund, D.M. Hallman, C.R. Perrey, C.B. Carter, A. Bapat, U. Kortshagen and W.W. Gerberich, Acta Mater. 54 (2006) p.4515.
[22] W.W. Gerberich, W.M. Mook, C.B. Carter and R. Ballarini, Int. J. Fract. 148 (2007) p.109.